Numerical and Experimental Analysis of a Slingsby Firefly Light Aircraft

Ana Filipa Oliveira das Neves
ana.das.neves@tecnico.ulisboa.pt

Instituto Superior Técnico, Universidade de Lisboa, Portugal

November 2019

Abstract

The purpose of this paper is investigating the stall characteristics of a light aircraft, more specifically the Slingsby Firefly T67M260. The objective was to obtain critical angle of attack, maximum lift coefficient, flow patterns visualisation of the boundary layer separation and vortex shedding frequency.

In order to accomplish these objectives, both Computational Fluid Dynamics and flight tests were performed. The RANS $k-\omega$ SST turbulence model was applied to half-model of the aircraft and a range of angles of attack were studied, pre and post-stall angles of attack. These flow calculations allowed for the identification of the critical angle of attack and respective maximum lift coefficient and for the observation of the separation pattern of the boundary layer on the upper surface of the wing. In addition, Detached-Eddy Simulations, with $k-\omega$ SST, were performed for the stall condition and post-stall with the objective of computing the vortex shedding frequency. This was accomplished by monitoring the static pressure at several probes in the wing's wake and the lift coefficient.

In order to evaluate the quality of the results, several flight tests were performed. Straight and level flights were performed at different speeds in order to compute the lift coefficient of the aircraft as a function of the angle of attack. In addition, wool tufts were implemented on the upper surface of the wing to visualise the pattern of the flow separation. Moreover, the aircraft was stalled and the buffet frequency was recorded with accelerometers inside the cockpit in order to compare it with the vortex shedding frequency.

Keywords: Stall, Aircraft, CFD, Vortex Shedding, Flight tests.

1. Introduction

Stall and Spin have received continuous attention from the aeronautical industry since the early flight days [1]. Spin is an autorotating descent in an helical pattern about the vertical axis. In order for this to occur the aircraft must be stalled, i.e. the critical angle of attack is exceeded. The critical angle of attack is the angle after which the aircraft has loss of lift. This is due to the boundary layer separation on the upper surface of the wing. Usually, before stall occurs a natural stall warning takes place, buffet. Buffet results from the separated flow of the wing, and its frequency is important due to the structural requirements. The complex separated flow, which is still poorly understood owing to its unsteadiness and three-dimensionality, and configuration dependence related to stall often result in a design challenge. The stall characteristics of an aircraft are required to comply with the regulations in order for it to be certified. However, these depend on several components of the aircraft and the study of the aircraft as a whole is done in the flight tests. The flight tests are performed in a later stage of the design of an aircraft, thus performing changes to comply with the stall requirements are often costly and might be too late to be implemented [2]. Hence, it is of utmost importance that the stalling of an aircraft is understood from an aerodynamics and dynamics point of view.

The wing of an aircraft is the main component that affects how a stall will develop, for instance how the flow separation propagates. The design usually begins by defining the wing planform and aerofoil section(s) used, and the structural requirements. In addition, knowing the maximum lift coefficient and critical angle of attack is of utmost importance.

The mentioned stall characteristics used to be understood with the data gathered from theory, wind-tunnel testing and flight tests however recently Computational Fluid Dynamics has also started to be utilized as a design toll. Although, wind-tunnel testing allows for a greater range of flight envelope to be tested it offers the disadvantage of representing high cost, it is time consuming and often the flight conditions are not met. Flight tests are only

performed in a later stage and it is not used as a design tool due to its tremendous cost and hazard to the test pilots. Ergo, CFD is gaining relevance and credit in the aeronautical industry due to its lower cost when compared to the available tools and for giving information of the flow properties in all the far field [3]. Nevertheless, this does not mean that wind-tunnel and flight test should be eliminated, but rather that CFD should be used as an additional tool. Nonetheless, it has limited accuracy hence it should be applied carefully.

This work aims at investigating important factors that will ultimately affect the stall of an aircraft, by studying a light aircraft, the Slingsby Firefly. This aircraft was chosen due to the existence of an accurate IGS file and the possibility of performing flight tests in order to validate the results obtained.

The main objective of this project is to evaluate he application of CFD, more specifically a widely used steady RANS turbulence and a very hybrid RANS/LES model, as an early design tool for the design of an aircraft. In order to do so the critical angle of attack, maximum lift coefficient, boundary layer separation pattern in the upper surface of the wing and vortex shedding were obtained with CFD and evaluate the results with several flight tests.

2. Methodology

2.1. Computational Fluid Dynamics of the Slingsby Firefly

1. Slingsby CAD Model

A Slingsby Firefly CAD Model was given by Cranfield University in a Initial Graphics Exchange Specification (IGES) format. The CAD model represented accurately the Slingsby Firefly aircraft. The model had sliver surfaces and intersecting geometry and in order to have a good meshing process a clean geometry is needed. Hence, the model was improved with the aid of the Space Claim ANSYS Software. The model given and the improved one are shown in figure 1. Only half of the model was meshed due computational resources available.

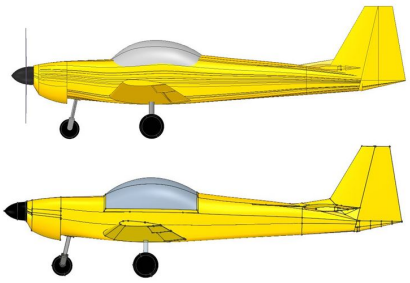

Figure 1: Original (Top) versus optimized geometry (Bottom).

The propeller was removed from the model since its effect on the flow was not to be analysed, the control surfaces remained due to their relevance to the stalling of the aircraft. Prior to the meshing phase the model requires checking. The 'Clean Topology' tool allows the user to understand if the geometry is represented correctly, i.e. if there are no curves unattached to a surface. If the geometry is all in red and blue after this is applied then the meshing process can be started, see figure 2.

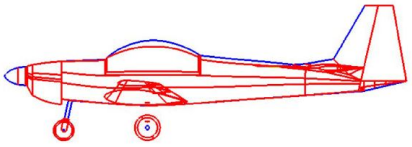

Figure 2: Topology of the Slingsby Firefly model.

2. Computational Domain

In addition, the computational fluid domain ought to be generated. The computational domain adopted for the flow calculations was a semi-cylinder described in a Cartesian coordinate system (x, y, z). Due to the boundaries conditions applied, there is a requirement that the domain ought be large enough so that the boundaries conditions can be met. Hence, it is advised that the domain size is typically 10 times the largest characteristic length of the body being studied. The largest characteristic length is the fuselage length (L). The domain possesses an inlet, outlet, far field and symmetry plane. Thus, the inlet distances 10L from the aircraft, the outlet 15L and the radius of the cylinder is 5L. The applied fluid computational domain schematic is shown in figure 3.

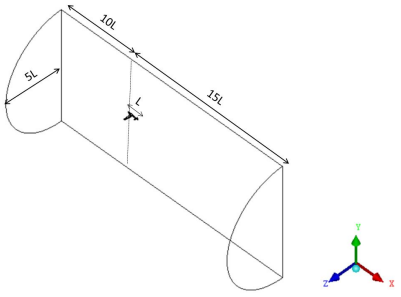

Figure 3: Isometric view of the computational fluid domain.

3. Meshing Process

An unstructured mesh was generated first with a top-down approach Octree method which means that it does not need any initial surface mesh and use the volume meshing distribution to impose a surface mesh onto the geometry and boundaries.

Due to the viscous nature of the flow, prism layers were then computed in order to represent the boundary layer. The final mesh was computed with the Delaunay method, a bottom-up approach which requires an initial surface mesh. The surface mesh is composed of triangles, the boundary layer with prisms and the volume mesh with tetrahedra.

An unstructured mesh allows for a rapid local mesh refinement exercise for both RANS and DES flow calculations. This type of mesh provides a rapid generation of a mesh for complex geometries and also allows for the generation of a density region. According to Spalart [4], there are several mesh regions with different densities. In this particular work, the region of interest is the wing's wake where the vortex shedding is computed. This is the focus region where nearly isotropic cells are required in order to in to resolve unsteady and time-dependent features. Hence, a density region with near isotropic cells is generated, with a grid spacing (Δ) of 0.03 m, which is approximately 2.5% of the mean aerodynamic chord, shown in figure 4.

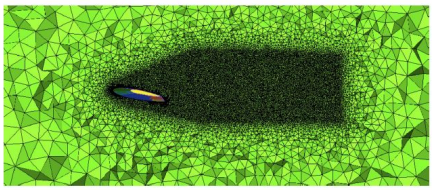

Figure 4: Detached-Eddy Simulations focus region.

The Reynolds number is $2.3 \cdot 10^6$, hence the assumption of a turbulent boundary layer. The boundary layer thickness (δ) is computed with equation: $\delta \approx \frac{0.37x}{Re^{\frac{1}{5}}}$ and it has a value of 0.024 m. Prism layers were generated in order to accurately represent the boundary layer. A initial height and total height were set so that the three regions of the turbulent boundary layer, viscous layer, buffer layer and log-law region were modelled . Hence, a dimensionless wall distance of $y^+ < 1$ and a total height that represented 20 % ($\delta^+ = 0.2$) of the boundary layer were imposed in the prisms generation. The reasoning for choosing to represent the 20% of the boundary layer was based on the profile of the turbulent boundary layer by Brederode [5], that states that after this value the outer layer is present. In the meshing software ICEM CFD, the desired y^+ is obtained by defining the first cell height (Δ_{y_1}) and number of prism layers (N) that ultimately will define the total height ($y_{(\delta^+=0.2)}$). Ergo, the number of prism layers (N) was 22 with a geometric growth factor of 1.2, with first cell height of $9 \cdot 10^{-6}$ and a total height of 0.0047 m. After applying all these parameters and computing the prism layer, a contour of the dimensionless wall distance in the upper surface of the wing was obtained and it is shown in figure 5. It is observed the the mean y^+ is below 1 as required. The summary of the boundary layer parameters computes is shown in table 1.

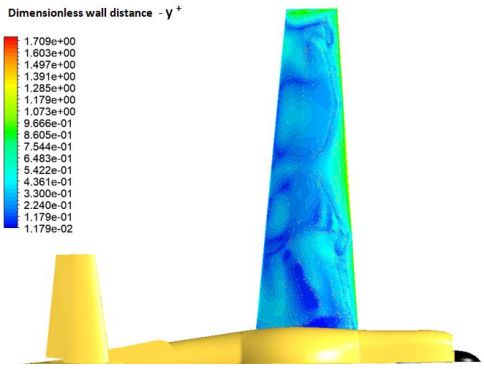

Figure 5: Dimensionless wall distance contour.

Table 1: Boundary layer parameters.

Re	δ	$\delta^+ = 0.2$	C_f	τ_w	u_τ	Δ_{y_1}	N
$2.3 \cdot 10^6$	0.024	0.0047	0.0031	1.664	1.256	$9 \cdot 10^{-6}$	22

4. Numerical Solving

ANSYS Fluent was the software used the numerical calculation of this project and it is widely used by the industry. There was the application of two different mathematical models: RANS two-equation turbulence model $k-\omega$ SST and Detached-Eddy Simulation model (DES). The use of two distinct models was based on acquiring different flow properties. The RANS model chosen was based on literature review since it was concluded to better predict highly separated flows [6],[7]. It was applied in steady state with the aim of obtaining the values of Lift and Drag, and the flow separation pattern on the upper surface of the wing. The Detached-Eddy Simulation model was chosen to find the shedding frequency of the wing's wake, since it is an unsteady phenomena. The numerical settings applied to both steady and unsteady simulations are shown in table 2.

Table 2: ANSYS Fluent numerical settings.

Numerical Setting	
Solver	Density-based
Solution methods: Formulation	Implicit
Solution methods: Flux Type	Roe-FDS
Spatial Discretization	
Gradient	Green-Gauss node based
Turbulent Kinetic Energy	Second order upwind
Spatial Discretization: Specific Dissipation rate	Second order upwind

The CFD model possess five boundaries: inlet, outlet, far field, symmetry plane and the aircraft model. The flow direction is $(1, 0, 0)$, i.e., in the

positive x direction. At the inlet, outlet and far field, pressure far field boundary conditions were applied. At the symmetry plane located at $z = 0$, symmetry conditions were applied. At the aircraft surface due to the no-slip and impermeability, the wall boundary condition was applied.

The set-up of the pressure far field boundary condition requires the free stream Mach number (M), flow Cartesian components, temperature and gauge pressure to be set. The Mach number was defined with the sound speed value at 5000 ft and has a value of 0.095. The flow direction is in the x direction, the angle of attack could be defined by the flow components. However, due to to the errors associated with the flow-cell distortion effect, the author decided to generate a different mesh for each angle of attack. Hence, the flow direction is always with the Cartesian components: (1,0,0). The gauge pressure is zero: "...for low Mach number flows (M $<$ 0.3), the 'Operating Pressure' is set as the ambient atmospheric pressure and therefore the gauge pressure can be set to zero." [8].

2.2. Flight tests

1. Straight and Level flight test

The first flight test was performed at a straight and level (unaccelerated) flight in which the aircraft was flown at different constant airspeeds. The altitude is maintained constant, in this case 5,000 ft. This test allowed for different angles of attack to be obtained and respective Lift and Drag. The lift slope was obtained by computing the lift coefficient and the wing's angle of attack by monitoring the power setting in instruments panel with and an inclinometer, respectively.

The quantities monitored were the airspeed, the rotations per minute (RPM) and the manifold pressure. The airspeed indicates the speed of the aircraft and it is shown in knots, the RPM are the rotations of the engine shaft and the manifold pressure (measured in inches of mercury) which measures the pressure inside induction system of the engine. A camera was used to record the gauges that measure this quantities: the Airspeed indicator, the tachometer and the manifold pressure gauge.

In addition, an inclinometer was used during the flight test and the angle was monitored with an additional camera. The inclinometer was positioned inside the cockpit close to the canopy, represented by the green line in figure 6, reading the angle ϕ. The value of the angle measured when the aircraft was stationary. The values read in the inclinometer were then transformed in the angle of a reference line in the fuselage, β, see blue line in figure 6. This reference line was present in the CFD model hence a validation of the CFD results could be performed. There is a difference of 5.5° between them. The AoA is defined as the angle between the mean aerodynamic chord and the flight path. The wing AoA has a difference of 5.63 ° to the angle β, according to the CAD model.

The Thrust (T) which is balanced by the Drag (D) was computed with the power settings of the aircraft. The weight is balanced by the lift (L), hence L was defined with the total weight minus the vertical component of thrust due to the AoA. The data processed from the flight test is shown in table 3.

Figure 6: Aircraft reference lines.

Table 3: Post-processed data from steady and level flights.

IAS (knots)	AoA (°)	T (N)	L(N)	D(N)
120	2.44	1962.015	9637.12	1960.74
100	3.45	1991.165	9601.01	1988.29
80	5.42	2287.15	9506.66	2278.27
70	9.56	1931.58	9399.50	1906.79
62	10.17	1844.48	9394.04	1817.57
60	11.27	448.46	9623.19	440.37

2. Stall angle of attack flight test

The α_{stall} was obtained with a different flight test due to the previous flight test only accounts for the pre-stall condition of the aircraft. The aircraft was stalled at a constant deceleration rate and engine idle, maintaining a straight and level flight.

In order to compute the α_{stall}, a camera mounted inside the cockpit recording the instruments panel, an inclinometer and an iPad with the software Airbox RunwayHD were used. The camera was recording the artificial horizon gauge that shows the pitch attitude hence obtaining the pitch angle (θ), the vertical speed indicator and altitude. The software used is a GPS that logs both the altitude and ground speed. It can be stated that one could used the Airspeed indicator to obtain the aircraft speed, however due to the increase angle of attack the air speed indicator is not reliable. This is owing to the pitot tube is no longer aligned with the flow,thus the airspeed indicator is actually showing a lower speed than it is in reality. Unfortunately, the data from the inclinometer was not perceptible due to the atmospheric conditions that did not allow for the screen to be seen.

The aim was to compute the flight path angle (γ) with both the vertical and horizontal speed thus ob-

taining the angle of attack with the pitch attitude angle. The pitch angle (attitude) is the angle between longitudinal axis and the horizon. The AoA is obtained by the difference between the pitch angle and the flight path angle. Although the inclinometer was positioned at the same reference line as the previous flight test in order to validate the flight tests, the video imagery was not perceptible.

3. Flow visualisation test with wool tufts

In order to be able to identify the boundary flow separation patterns in the upper surface of the wing, flow visualisation techniques in-flight were required. The most suitable flow visualisation techniques to detect flow direction and boundary layer separation are either flow cones and tufts or emitted fluid technique. The wool tufts visualisation technique was chosen due to the its practicality but also for being a standard method of flow visualisation.

Ergo, the second flight test consisted in the observation of the boundary layer separation progression with wool tufts on the upper surface of the wing. The wool tufts are placed in the boundary layer and one should expect the wool tufts to remain aligned with the flow and undisturbed when the aircraft is not approaching stall. When the aircraft is stalled the boundary layer will begin to separate and the wool tufts will possess a disturbed behaviour in the sense that they will not be aligned with the flow direction.

The left wing of the Slingsby Firefly was covered by wool tufts of 15 cm length. A structured pattern was implemented, i.e., the tufts were vertically and horizontally spaced 24 cm. This structure was based on the work developed by Hoff [9], in which this structured allowed for the observation of several patterns upon spinning an aircraft. Due to the fuel tank and taper of the wing some of the tufts were reduced in length and spacing in order to be able to cover most of the wing upper surface. The tufts schematic is shown in figure 7, the green arrows represent the spacing and the blue the length of the wool tuft. This resulted in 62 wool tufts that were attached to the upper surface of the wing with paper tape. There was a camera installed inside the cockpit with a a view towards the wing.

4. Buffet Frequency flight test

Approaching stall there will be a vibration of the aircraft known as buffet, resultant from the separated flow. In the cockpit three sensors were mounted in three different locations shown in figure 8. The available sensors were the Shimmer3 which have an accelerometer, magnetometer and a gyroscope. The vertical acceleration was analysed in order to compute the buffet frequency induced by the vortex shedding of the wing's wake. The data frequency acquisition was 100 Hz and a Fast Fourier Transform (FFT) was implemented in order to convert the signal in the time domain to the frequency domain.

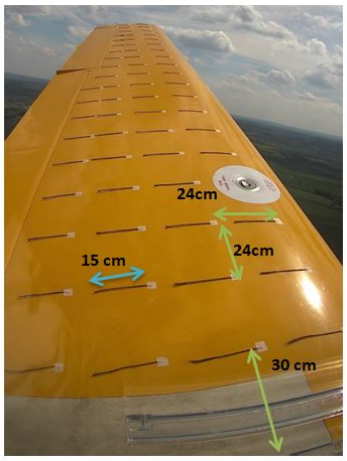

Figure 7: Wool Tufts Scheme.

Figure 8: Sensor's position inside the cockpit

3. Results

A mesh sensitivity analysis was performed with three mesh densities (coarse, medium and fine) in order to understand which mesh density would be suitable to perform all the flow calculations based on the physical accuracy and computational time. The medium mesh revealed to be the best choice, hence all the following results were obtained with flow calculations with a medium mesh.

3.1. **Lift Curve, critical angle of attack and maximum lift coefficient**

The lift coefficient as a function of the AoA (relative to the mean aerodynamic chord of the wing), obtained from the CFD calculations using the steady RANS turbulence model $k-\omega$ SST and the mathematical model DES with $k-\omega$, is shown in figure 9. The range of AoA studied are from 5-20 ° with a 2° interval for the steady flow calculations and the AoA= 14, 16 and 18 ° for the DES.

The lift curve obtained from the steady RANS calculations has two distinct regions: a region where a linear behaviour is observed up until a certain

angle is reached, i.e., a maximum angle that corresponds to the maximum lift coefficient, and a region after which the increase of angle of attack no longer produces more lift.

The first region (AoA = 5-14°) corresponds to an approximately linear variation of lift, this means an increase in α would result in a direct increase in lift. The linear curve is defined by : $C_L = 0.0845\alpha + 0.0734$, this means that $dC_L/d\alpha \approx 0.0845$ and that the zero lift angle is ≈ -0.87 °. The lifting-line theory gives a lift coefficient of 0.0898, giving a deviation of the ≈ -6% of the CFD results obtained with the RANS turbulence model, $k-\omega$ SST. The lifting-line theory only accounts for the lift of a finite wing, whereas the CFD model has the influence of other components, hence the lift slope of the CFD results ought slightly different from the lifting line theory slope.

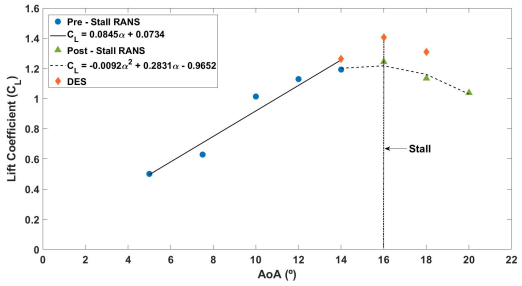

Figure 9: Lift Coefficient obtained from steady RANS $k-\omega$ SST and DES with $k-\omega$ SST flow calculations as a function of the AoA.

This linear behaviour of the lift coefficient no longer applies after the critical angle of attack is reached, which corresponds to the maximum lift coefficient. For the mentioned results, the values of α_{stall} and C_{Lmax} are respectively 16° and 1.25.

The second region of the curve corresponds to the post-stall conditions after which increasing the angle will no longer produce more lift. At this stage the flow is massively separated, and during flight this results in a wing or nose drop. For a trailing-edge stall a gradual loss of lift should be expected in this region. In fact from the critical angle of attack up to AoA = 20 ° there is a decrease of 0.206 in the value of the lift coefficient, it is concluded that there is a gradual loss of lift.

The DES values of lift coefficient are also presented in figure 9. Due to the computational time required for the DES flow calculations, which took five days in order to have one second of flow time calculated, the averaging of flow was started after one flow passage. The results presented are from an averaged flow passage. The total flow time simulated was two flow passages, which corresponds to 11 seconds of flow time. The residuals dropped to 10^{-5} in each time step, which according to ANSYS guidelines is sufficient to obtain convergence in each time step. Hence, DES was only applied to the AoA = 14, 16 and 18 ° due to time available for this project and the AoA for which buffet would occur. The values of the lift coefficient are higher for the DES than the RANS solutions. For the AoA studied with DES the flow is highly separated and unsteady, hence the RANS model fails to accurately predict the lift coefficient. Since DES accounts for the unsteadiness of the flow and different scales of turbulence, it should be expected values of the lift coefficient closer to the flight test values.

These results were compared with the flight tests results, more specifically the straight and level and stall angle flight tests. The lift curve obtained from the flight tests showed a linear behaviour, this was expected since the AoA reached during the flight tests were only in the pre-stall condition. The best fit curve for the lift was: $C_L = 0.0939\alpha + 0.0674$, with α in degrees. If it is assumed that the linear behaviour of the C_L remains up to the AoA=16°, the α_{stall} obtained from the CFD calculations, the maximum lift coefficient is 1.57. The zero lift angle is -0.7 °.

In table 4, the slope of the lift curve (a) and zero lift angle (a_0) are shown. In addition, the best fit curves are also presented. The steady RANS solutions have a lift curve slope that differs 10 % from the lift slope obtained from the flight tests and zero lift angle is 20% lower for the CFD calculations. This results in a general under prediction of the lift coefficient obtained from the CFD flow calculations. In addition, for the DES results the lift coefficient is closer to the flight tests. This under prediction could be improved by modelling the propeller in the CFD calculations.

Table 4: Summary of the results of CFD and flight tests.

Data set	α_0	$a(C_L/^\circ)$	$\alpha_{stall}(^\circ)$	C_{Lmax}	Trendline equation
CFD Pre-Stall - RANS	-0.87	0.0845	-	-	$C_L = 0.0845\alpha + 0.0734$
CFD Post-Stall - RANS	-	-	16	1.24	$C_L = -0.0092\alpha^2 + 0.2831\alpha - 0.9652$
CFD - DES	-	-	16	1.40	-
Flight tests	-0.72	0.0939	16*	1.57*	$C_L = 0.0939\alpha + 0.0674$

* Assuming a linear curve until the critical AoA=16 °.

The critical angle of attack flight test was performed and a critical AoA of 18 ° was found, see figure 10. Due to the propeller slipstream that has a destalling effect, it was expected a flight critical angle of attack higher than the one computed with CFD.

3.2. Boundary layer flow separation visualisation

Contours of the limiting streamlines were obtained to visualise the boundary layer flow separation mechanism in the upper surface of the wing. They

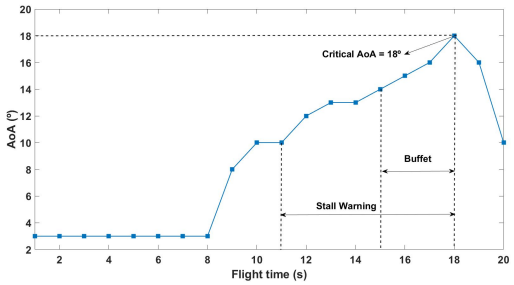

Figure 10: AoA as a function of flight time of the critical stall flight test.

are the lines tangent to the shear-stress vector at the wall. They allow the detection of attached and separated flow which is highly important to understand the flow separation pattern. The results of those contours for the AoA studied are shown in 12.

Figure 11: Streamlines of the different AoA.

The Slingsby Firefly has a tapered wing with washout, i.e., the angle of incidence at the root is higher than at the tip. As the angle of attack is increased the flow begins to separate at the root due to its washout. Further increase of the AoA will result in an increase of flow separation in both spanwise and chordwise directions. The aerofoils used in the wing are both thick aerofoils hence a trailing-edge stall is present. This mean that the flow will separate first at the trailing-edge and move towards the leading-edge as the angle of attack increases. This progression of flow separation is shown in figure 12.

The results were compared with imagery from wool tufts visualisation in-flight. The boundary layer flow separation patterns and progression is similar to the one encountered in the CFD tests. The localization of the patterns found are also similar between the CFD and flight test results. Figures 12, 13 and 14 show some of the AoA wool tufts imagery with the respective streamline contour.

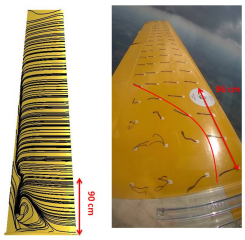

Figure 12: Flow visualisation of the flow with an AoA of 10 degree and equivalent flight test image.

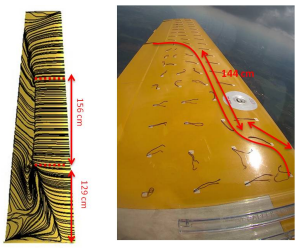

Figure 13: Flow visualisation of the flow with an AoA of 14 degree and equivalent flight test image.

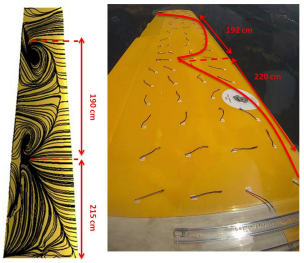

Figure 14: Flow visualisation of the flow with an AoA of 18 degree and equivalent flight test image.

3.3. **Vortex shedding frequency**

The hybrid RANS/LES model, DES with $k-\omega$ SST, was implemented after a converged RANS solution of the α=14,16,18° was obtained. Due to time concerns, there was a decision of only applying this model to the AoA where buffet occurred (AoA = 14, 16 and 18 °) in order to compare the vortex shedding frequency with the buffet frequency measured in the flight tests.

The results obtained from the CFD calculations were compared with the buffet frequency of the aircraft when approaching stall. Buffet results from changes in pressure resulting in an airframe vibration, hence the reason for monitoring the static pressure (P_{static}) at several points in the wing's wake. In the addition, the changes in pressure are responsible for variation on the lift force, since the pressure acts perpendicular to the wing's surface. During flight, buffet is the structure response to the periodic changes in lift. Hence, the buffet frequency ought to be similar to the frequency of the static

pressure ($f_{P_{static}}$) wing's wake and lift coefficient.

The FFT was applied to the static pressure for the points monitored and to the lift coefficient of the three AoA studied. The time step used was 0.00067s which corresponds to a frequency of acquisition of 1472 Hz. The data presented are from four points at different regions in the wake of the wing for the three AoA.

The author carefully chose four different points situated at different regions in the wing's wake in order to capture the frequency of the vortex shedding at different locations. The points chosen were P5, P10, P14 and P15 and are shown in figure 15.

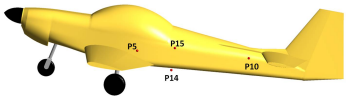

Figure 15: Lateral view of the probes.

The FFT of the data of the probe 5 is shown in the graph 16. It is observed that a dominant peak exists which corresponds to the dominant shed structures frequency, i.e., the vortex shedding frequency. In addition, other smaller peaks at higher and lower frequencies were present. The several peaks found were expected due to the different length scales turbulent flow possess. Since the probes monitored were in the region where LES is activated (focus region), different frequencies ought to be captured. The lower frequency peaks occur due to the presence of large eddies (low frequencies) that are the biggest contributors for the turbulence kinetic energy and the higher frequency peaks the smaller eddies. For the same AoA the frequency remains unaltered in the different probes. Furthermore, an increase in the AoA results in a decrease in the f_{vs}. The lift coefficient was also monitored and the respective results are shown in table 5.

Table 5: Summary of the f_{vs} (Hz) of the probes: P_5, P_{10}, P_{14}, P_{15} and C_L for the AoA = 14,16,18 °.

AoA (°)	$f_{vs}P_5$	$f_{vs}P_{10}$	$f_{vs}P_{14}$	$f_{vs}P_{15}$	$f_{vs}C_L$
14	11.66	11.66	11.66	11.66	11.74
16	10.2	10.2	10.2	10.2	10.19
18	8.946	8.742	8.946	8.946	8.742

In order to evaluate the quality of the previous results, the buffet frequency was measured in flight with accelerometers. The aim was to compare it with the shedding frequency obtained in the CFD flow calculations. The buffet had a duration of 3 seconds before the wing dropped, two stalls were performed and data was recorded for both. Those 3 seconds of data were analysed and a Fast Fourier Analysis was performed in order to obtain the buffet

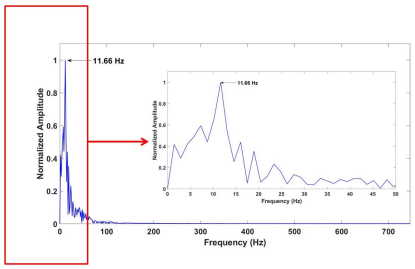

(a) **AoA = 14°**

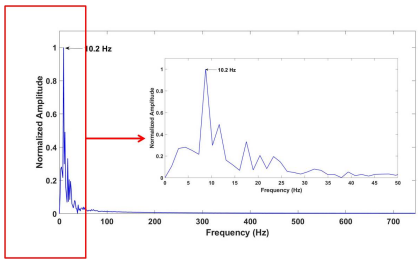

(b) **AoA = 16°**

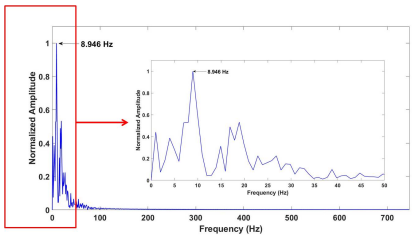

(c) **AoA = 18°**

Figure 16: FFT analysis of P_{static} at point P5 for the different AoA studied .

frequency. The acquisition frequency was 100 Hz and the amplitude was normalized.

A detailed analysis was performed to the data from sensor n^o3, in order to verify if the increase in angle of attack would result in a decrease of the buffet frequency, as it was what was observed with the CFD flow calculations. In fact, that was observed and it is shown in figures 17, 18 and 19. The different peaks in the FFT are due to the signal noise from several sources of the aircraft. A filter could be applied to eliminate the noise in the signal, however accurately applying a filter without damaging important data is a challenge and should be performed carefully.

The AoA studies performed with CFD corresponded to the same AoA reached in the flight test. Owing to this, the results obtained can be compared qualitatively and quantitatively. In table 6, the CFD and flight test results for the frequency of the vortex shedding and its relative deviation are presented. In addition, the Strouhal number (St), based on the projected height, $h = \overline{c} \cdot sin(\alpha)$, was computed for the CFD and flight test results. The values of St varied from 0.1-0.115, which is typical

for unswept wings with flow separation (S=0.1-0.2).

The relative deviation between the flight test and the monitored quantities is below 3% for all the conditions presented. Hence, considering all the simplifications in the CFD model and flight test errors, the results are promising.

Table 6: Percentage of the relative error of the quantities frequency: P_{static}, and C_L.

AoA	$f_{Flight\ test}$ (Hz)	$f_{P_{static}}$ (Hz)	$\lvert\Delta_{rel}\rvert_{P_{static}}$ (%)	$f_{(C_L)}$	$\lvert\Delta_{rel}\rvert_{C_L}$ (%)	$St_{Flight\ test}$	$St_{P_{static}}$	St_{C_L}
14	12	11.66	2.83	11.74	2.17	0.115	0.111	0.106
16	10.16	10.2	0.39	10.19	0.3	0.111	0.105	0.105
18	9	8.946	0.6	8.742	2.87	0.110	0.103	0.10

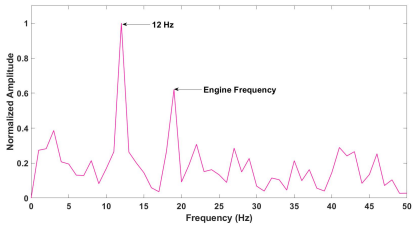

Figure 17: Fast Fourier Analysis of 1st second of stall (sensor n°3).

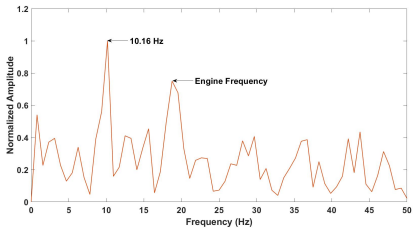

Figure 18: Fast Fourier Analysis of 1st second of stall (sensor n°3).

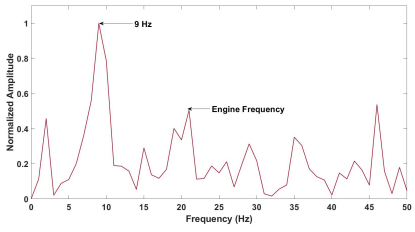

Figure 19: Fast Fourier Analysis of 1st second of stall (sensor n°3).

4. Conclusions

The thesis addresses the stall characteristics of a light aircraft, the Slingsby Firefly, more specifically the critical AoA and correspondent maximum lift coefficient, the patterns of the boundary layer flow separation on the upper surface of the wings for the pre and post stall conditions and finally the vortex shedding frequency that results in a vortex induced vibration, buffet. This last parameter is important from both an aerodynamic and structural point of view.

The above mentioned characteristics were computed numerically with the application of CFD. The mesh of half of the model of the Slingsby was computed with the commercial software ICEM CFD. The CFD flow calculations were performed with a steady RANS turbulence model $k\omega - SST$ and Detached-Eddy Simulation, with commercial solver ANSYS Fluent. The results obtained from the numerical calculations were qualitatively and quantitatively (with the relative deviation) evaluated with several flight tests performed.

Three different meshes with distinct densities (coarse, medium and fine mesh) were computed and their respective numerical calculation was performed for a Pre-Stall AoA = 12 ° and a Post-Stall AoA = 18°. This was done in order to understand which mesh would be suitable to perform all the flow calculations based on the numerical and physical accuracy and the computational time required. The quantities monitored were both the lift and drag coefficient, the pressure distribution for three different section on the wing and the limiting streamlines contour for the AoA mentioned. Overall, the medium mesh presented the best physical accuracy with a computational time reduced compared to the fine mesh. Ultimately, the medium mesh density was applied to all the flow calculations.

The steady RANS flow calculations with the turbulence model $k - \omega$ SST were carried out for the AoA = 5, 7.5, 10, 12, 14, 16, 18 and 20 °. The lift curve obtained showed that the pre-stall condition of the aircraft occurred up to the AoA = 14°. The pre-stall region showed a linear behaviour, as it was expected. The best fit curve was: $C_L = 0.0845\alpha + 0.0734$, which gives a zero lift angle of -0.87 °. The lift slope of the numerical simulations have a -6% deviation from the lifting line theory curve. Due to the non-existence of the propeller, which augments lift over the section of the wing due to the slipstream, in the CFD model, the lift coefficient in the pre-stall condition was under predicted when compared with the steady flight test, which had a linear curve with the following equation: $C_L = 0.0939\alpha + 0.0674$, giving a zero lift angle of -0.7 °. The post-stall region had a critical angle of attack of 16 ° and a maximum lift of 1.25. A flight test to obtain the critical angle of attack was performed and the value found was 18 °, which is two degrees higher in comparison with the CFD results due to the destalling effect of the propeller. The post-stall region had the highest de-

viation of the C_L, since close to the critical angle of attack the boundary layer flow on the upper surface of the wing is separated, which is an unsteady phenomenon that the steady RANS doe not account for. Hence, the DES values of lift which account for the lift variations are expected to give closer C_L results to reality, however the post-stall region was not accounted in the flight tests. The drag coefficient was also obtained from the CFD flow calculations. However due to the interaction of the different bluff bodies during flight, which due to the mesh density used were not modelled in the CFD model, the results could not be compared to the flight test results. Nevertheless, for a CFD model that lacks the propeller the lift curve slope and zero lift angle are in within a 10 % deviation, except for an angle of attack. Moreover, the application of DES for AoA close to the critical angle will ultimately give a good approximation of the lift coefficient. Hence, the steady RANS calculations can define the pre-stall condition of the aircraft and the DES flo calculation the post-stall condition.

The flow separation patterns observed both with CFD and the wool tufts visualisation technique were similar. The patterns encountered were the same and their relative location in the wing as well. In an early design stage of an aircraft, where unsteady solutions of the flow are not possible, steady RANS flow calculations using the turbulence model $k-\omega$ SST can be performed in order to understand how the flow separation propagates in the wing surface. These findings are important because the flight tests are often costly and performed in a later design stage, hence at a low computational cost the flow separation mechanism can be performed.

The DES performed in converged solutions of the stall and post-stall conditions proved to predict the vortex shedding frequency accurately when compared to the buffet frequency measured during flight. This is important in order to understand the limitations of the structure of the aircraft due to the vibrations induce by the buffet.

To sum up, the work developed allows for the characterization of important stall characteristics, with a medium mesh density and CFD mathematical models, that are usually only possible to obtain with flight and wind tunnel testing. This allows for a better understanding of the stall characteristics of an aircraft, thus reducing the costs of later alterations on the design when only flight tests were available. Moreover, the first stage of a spin is a stalled aircraft hence the present results can aid the description of the spin of the Slingsby Firefly.

Acknowledgements

The author would like to thank Professor Nicholas Lawson and Professor Luís Eça for all of their support and guidance in this project and also for giving me the opportunity to work with them.

References

[1] J.R. Chambers and H. P. Stough. Summary of NASA Stall/Spin research for general aviation configurations. In *AlAA General Aviation Technology Conference. Anaheim, CA, 29th September-1st October 1986.*, volume AIAA-86-25, Reston, VA. AIAA, AIAA-86-2597.

[2] Mcveigh M. A. and Kisielowski E. A design summary of stall chracteristics of straight wing aircraft. Technical report, NASA, Washington D.C, June 1971.

[3] Edward Tinoco. The changing role of computational fluid dynamics in aircraft development. In *16th AIAA Applied Aerodynamics Conference, Albuquerque,NM,U.S.A., 15 - 18 June 1998*, Reston, VA. AIAA: AIAA-98-2512.

[4] P. Spalart. Young-person's guide to detached eddy simulation grids. Technical report, NASA, July 2001.

[5] Vasco de Brederode. *Aerodinâmica Incompressícel:Fundamentos*. IST Press, Lisboa, 1st edition, 2014.

[6] Florian Menter, M. Kuntz, and R Langtry. Ten Years of Industrial Experience with the SST Turbulence Model. *Heat and Mass Transfer*, 4, 2003.

[7] Di Zhang. Comparison of various turbulence models for unsteady flow around a finite circular cylinder at re =20000. *Journal of Physics: Conference Series*, 910:012027, 10 2017.

[8] N. Lawson. Ansys fluent user guide - 3d cfd solutions. National Flying Laboratory Centre, Cranfield Univerity, 2017.

[9] R.I. Hoff. *The Aeroplane Spin Motion and an Investigation into Factors Affecting The Aeroplane Spin*. Phd, Brunel University London, 2017.